MORPHODYNAMICS OF

SHOREFACE–CONNECTED RIDGES

A. FALQUES[1] D. CALVETE[1] H. E. DE SWART[2] N. DODD[3]

Abstract

A morphodynamic model is developed and analyzed to gain fundamental under-standing on the basic physical mechanisms responsible for the characteristics of shoreface-connected sand ridges observed in some coastal seas. These alongshore rhythmic bedforms have a horizontal length-scale of order 10 km. It is found that the positive feedback between the topographic disturbances of a sloping bottom and the subsequent deflection of the mean coastal current is the main cause of the ridges. To be effective, this mechanism needs an averaged sediment trans-port mainly due to wave stirring during storms and an averaged current driven by pressure gradients rather than surface stresses. Even in the presence of signif-icant tidal currents, their origin — related to the mean current instead of tidal oscillation — is essentialy different from that of tidal sand banks.

1   Introduction

Shoreface-connected ridges are elongated sand banks found in the inner part of some continental shelves in horizontal patterns with a length-scale of order O(10 km). Such ridges are present, for example, near the Dutch coast (see e.g. Van de Meene, 1994, and figure 1), near the east coast of the United States of America (Swift *et al.* 1985), near the Argentinian coast (Parker, Lanfredi & Swift, 1982). They start at the offshore end of the shoreface and they extend seaward forming an angle of $20^o - 35^o$ with respect to the coastline. In contrast with the

[1]Departament de Física Aplicada, Universitat Politècnica de Catalunya. 08034 Barcelona, Spain

[2]Institute for Marine and Atmospheric Research, Utrecht University. 3584 CC Utrecht, The Netherlands

[3]Coastal Group, HR Wallingford. OX10 8BA Wallingford, United Kingdom
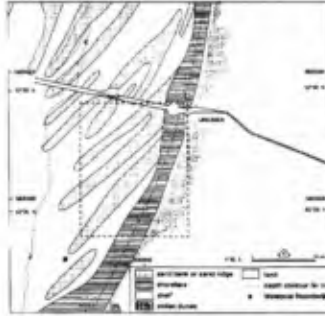
Figure 1: The dutch shoreface-connected sand ridges (Van de Meene, 1994).

more offshore tidal sand banks (see e.g. Hulscher, De Swart & De Vriend, 1993), their orientation is not cyclonically oriented with respect to the tidal current, but it is related to the alongshore mean coastal current, the seaward end of the ridge being shifted upstream with respect to its shoreface attachement. Hereafter we will refer to this as upcurrent rotated bars. The opposite orientation will be defined as downcurrent rotated.

The alongshore spacing between successive crests of shoreface-connected ridges ranges between 5 and 10 km. The length of individual crests is between 10 and 25 km. Their height is between 1 and 6 m in water depths between 4 and 20 m. The ridges slowly migrate in the direction of the dominant current with a celerity of a few $m yr^{-1}$.

In general, sand banks are important, since they may form shallow areas which are hazardous for shipping traffic and may affect the stability of pipelines and oilrigs, due to lateral movements. They are also possible sources for sand mining. The shoreface-connected ridges, which form the seaward boundary of the nearshore zone, play a relevant role in the dynamics of the coastal system (Van de Meene, 1994).

There is geological evidence that the ridges are not relict features, that is, they are active under the present hydrodynamic conditions and their growth has taken place during the Holocene. For instance, on the Dutch inner shelf they started to form about 3400 years ago. Therefore, as it is the case for many sea bed patterns an explanation of the origin of the ridges as an inherent free instability of the coupled bottom-fluid system under the action of some current seems plausible. Given a small disturbance of a simple reference topography (e.g., a flat bottom) the response of the flow to this perturbation can result in a sediment transport pattern which reinforces the bottom undulation. Then a positive feedback is induced and both disturbances will grow in time.

According to Trowbridge (1995), storms are the main cause of the currents capable of generating shoreface-connected ridges. Indeed, storm driven currents can be of order $0.5 - 1\ m s^{-1}$ in the areas where ridges are observed off the coast of Holland, Florida and Argentina. However, while tidal currents are rather weak on the American shelf, they are important near the Dutch coast $(0.7 - 1.1\ m s^{-1}$, at the surface). Also, as we will see, an important contribution from alongshore gradients on the free surface elevation can occur on the mean current.

Trowbridge (1995) studied the morphologic stability properties of a storm-driven alongshore current, with a cross-shore gradient, on a shelf bounded by a straight coast and with a transverse slope. It was shown that the system is unstable and leeds to the growth of bedforms very similar to the observed ridges. It was suggested that the basic physical mechanism was the offshore deflection of the flow over the shoals and the related loss of sediment carrying capacity in the offshore direction due to the transverse slope. However, a severe assumption in this model is the condition of irrotational flow. This implies that the production of vorticity due to bottom frictional torques and Coriolis terms, which has been proven to be very important for tidal sand banks dynamics (see Zimmerman 1981; Hulscher *et al.* 1993) is neglected. In addition, a crude sediment transport parametrization is used, where the sediment flux is assumed to be linear in the mean flow velocity and the downslope effect on the transport direction is not accounted for. As a result his model does not predict any preferred spacing between ridge crests. Furthermore, the model deals with linearized evolution equations just allowing for the initial growth of small amplitude solutions.

In this paper we investigate a generalized and physically more realistic model for both the water and sediment motion. The fluid is described by the full 2D shallow water equations, which include bottom friction and Coriolis terms. The sediment flux is assumed to be proportional to some power m of the current so that the role of different choices for m can be explored. Finally, a nonlinear extension of the model is briefly described and some preliminary results of finite amplitude evolution is presented.

2   Model formulation

2.1   Equations of motion. Scaling

As shown in figure 2, the inner shelf is schematized as a sloping sea bed, bounded by a straight vertical wall which represents the seaward end of the shoreface. Further offshore, a horizontal flat bottom describes the outer shelf. An orthogonal coordinate system is taken with the x, y and z-axes pointing in the cross–shore, longshore direction and vertical direction, respectively. The still water level is represented by $z = 0$. Although the vertical structure of the currents can have an important role in the ridge area, in view of earlier studies on large scale bedforms it is worthwhile to investigate whether a 2D model can describe the main characteristics of the ridges. Therefore, the fluid motions are considered to be governed by the 2D shallow water equations, which consists of the depth–averaged momentum equation and mass conservation equation. The bottom evolution follows from the sediment conservation equation.

In order to make the equations of motion dimensionless we now introduce characteristic magnitudes L_H, L_V and U for the horizontal length, the depth and the current. L_H is the width of the inner shelf, L_V and U are typical values of the water depth and the mean current. For example, representative values for the Dutch inner shelf are $L_H \sim 12 \times 10^3$ m, $L_V \sim 15$ m and $U \sim 0.25$ m s^{-1}. The variables are made dimensionless as follows:

$$(x, y) \to L_H(x, y) \quad z_b \to L_V z_b \quad v \to Uv \quad t \to T_m t \quad z_s \to \frac{U^2}{g} z_s . \quad (1)$$
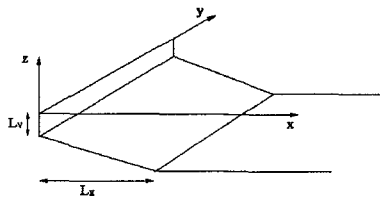
Figure 2: Sketch of the geometry and the coordinate system.

The scaled momentum and mass conservation equation read:

$$\epsilon \frac{\partial v}{\partial t} + (v \cdot \nabla)v + \hat{f} \times v = -\nabla z_s + \frac{\tau}{D} \qquad (2)$$

$$\epsilon \frac{\partial D}{\partial t} + \nabla \cdot (Dv) = 0 \qquad (3)$$

and the sediment conservation equation read:

$$\frac{\partial z_b}{\partial t} + \nabla \cdot q = 0 \,. \qquad (4)$$

Here v is the current vector, $\hat{f} \times v$ is the Coriolis acceleration, τ represents the free surface and bottom stress terms ($\tau = \tau_s - \tau_b$). The free surface, the bottom and the total height of the water column are given by $z = z_s$, $z = z_b$ and D, so that $D = F^2 z_s - z_b$. The nabla–operator is defined by $\nabla = (\partial/\partial x, \partial/\partial y)$. The volumetric sediment flux per unit width is denoted by q. It is important to note that, since the growth of the ridges takes place on very long time scales ($O(10^3$ yr)), all the quantities in the governing equations have to be considered as averages over a long time $O(1$ yr).

The boundary conditions imposed for this system are periodic conditions in the longshore direction. Furthermore, at $x = 0$ (the transition shoreface-inner shelf) and for $x \to \infty$ we assume that the cross-shore flow component vanishes and the bottom elevation is fixed to its reference value.

In order to close the model parametrizations for the bed shear stress τ_b and the sediment flux q are required. We will consider a linear friction law and the volumetric sediment flux parametrized as

$$\tau_b = rv \qquad\qquad q = |v|^m \left(\frac{v}{|v|} - \hat{\gamma}\nabla h \right) \,. \qquad (5)$$

The coefficient $\hat{\gamma}$ is related to the angle of repose of the sediment, so the term $-\hat{\gamma}\nabla h$ accounts for the tendency of sand to move downslope and m is an exponent which is usually between 1 and 6. Finally, h is the elevation of the bottom with respect to a specific equilibrium profile, to be discussed in the next subsection. Further details on sediment transport can be found in Van Rijn (1993) and Fredsoe & Deigaard (1993).

Two time scales appear which are defined as

$$T_h = \frac{L_H}{U} \qquad\qquad T_m = \frac{L_H L_V}{\nu U^m} \qquad (6)$$

The hydrodynamic time scale T_h follows from scaling the three equations (2)–(3) and the morphodynamic time scale T_m results from scaling equation (4). Here ν is the coefficient that multiplies the right hand side in the dimensional version of the sediment flux parametrization (eq. (5)). For simplicity, it has been assumed to be constant. Other parameters in the model are

$$\epsilon = \frac{T_h}{T_m} \qquad F^2 = \frac{U^2}{gL_V} \qquad \hat{f} = f_c\frac{L_H}{U} = Ro^{-1} \qquad r = r_*\frac{L_H}{UL_V} \qquad \hat{\gamma} = \gamma\frac{L_V}{L_H} \qquad (7)$$

The hydrodynamic timescale is assumed to be much smaller than the morphodynamic one. This allows for the adoption of the quasi-steady hypothesis, that is, the fluid instantaneously adjusts to the bathymetric changes. This permits to drop the time derivatives ($\epsilon \approx 0$) in the three differential equations (2)–(3). Using the scales of motion, it appears that the Froude number F is very small, $F \sim 0.02$. Consequently, in the forthcoming analysis the water column is assuumed to be equal to the bottom, $D = -z_b$.

2.2   Basic state

In this study we model the reference bottom profile as

$$H(x) = \left\{ \begin{array}{ll} 1 + \beta x & (0 \leq x < 1) \\ 1 + \beta & (x \geq 1) \end{array} \right. \qquad (8)$$

Note that $H(x)$ and x are dimensionless, and that the depth at the seaward end of the shoreface has been chosed as vertical length-scale, L_V. In case of the Dutch inner shelf, $L_V \sim 15$ m, $L_H \sim 12 \times 10^3$ m and the water depth on the outer shelf is ~ 20 m , so that $\beta = 0.33$.

It is easily seen that a steady basic state of the form

$$\boldsymbol{v} = (0, V(x)) \qquad\qquad z_s = \delta\, y + \xi(x) \qquad\qquad z_b = -H(x) \qquad (9)$$

where $\delta = g\, s\, L_H/U^2$ is the dimensionless parameter for the longshore gradient, s, is a solution of the governing equations (2), (3), (4) . The alongshore momentum balance between forces related to the longshore pressure gradient, windstress and bottom friction is achieved by

$$V = \frac{\tau_{sy} - \delta\, H}{r} \qquad (10)$$

It has been demonstrated by Scott & Csanady (1976) and Van der Giessen, De Ruijter & Borst (1990) that the momentum balance using the linear friction law (5) yields a good description of mean currents in the coastal zone.

Analysis of current data obtained on the East American inner shelf (Scott & Csanady 1976; see also Chase 1979) indicate that the sea surface slope $s \sim 1 - 2 \times 10^{-7}$ and the friction coefficient $r_* \sim 5 \times 10^{-4}$ m s^{-1}. Similar values appear to apply to the Dutch inner shelf. The physical mechanism causing the longshore pressure gradient is discussed by Chase (1979). Based on the field data discussed above we choose $\tau_{sy} \simeq -0.1$ Nm^{-2} and $s \simeq 2 \times 10^{-7}$. This yields an estimate of the longshore velocity scale: $U \equiv V(x = 0) \simeq 0.25$ m s^{-1}. Both the longshore windstress and pressure gradient are comparable and force a flow in the same, negative, y-direction.

Combining equations (8) and (10) and including the new parameter $a = |\delta|/r$, the velocity profile for the basic state reads:

$$V(x) = \begin{cases} \pm(1 + a\,\beta\,x) & \text{if } 0 \le x \le 1 \\ \pm(1 + a\,\beta) & \text{if } x > 1 \end{cases} \tag{11}$$

and the sign of the flow is determined by the direction of the applied wind and longshore pressure gradient forces. The parameter a measures the relative effect of the longshore pressure gradient in maintaining the basic state velocity. By using the definition of velocity scale U it follows that a can vary between 0 (no pressure gradient) and 1 (wind stress negligible).

2.3   Linear stability analysis

The formation of rhythmic bedforms can then be investigated by studying the dynamics of small pertubations evolving on this steady state:

$$z_s = \zeta + \eta(x,y,t) \quad z_b = -H + h(x,y,t) \quad \boldsymbol{v} = (0,V) + (u(x,y,t),v(x,y,t)) \tag{12}$$

where $\zeta = \delta\,y + \xi(x)$. The scaled linearized momentum (2) and mass conservation equation (3) read:

$$V\frac{\partial u}{\partial y} - \hat{f}v = -\frac{\partial \eta}{\partial x} - \frac{r}{H}u \quad , \quad V\frac{\partial v}{\partial y} + \frac{dV}{dx}u + \hat{f}u = -\frac{\partial \eta}{\partial y} - \frac{r}{H}v + \delta\frac{h}{H} \tag{13}$$

$$\frac{dH}{dx}u + H\frac{\partial u}{\partial x} + H\frac{\partial v}{\partial y} - V\frac{\partial h}{\partial y} = 0 \tag{14}$$

and the sediment conservation equation (4) reads:

$$\frac{\partial h}{\partial t} = -|V|^{m-1}\left\{ \frac{(m-1)}{V}\frac{dV}{dx}u + \frac{\partial u}{\partial x} + m\frac{\partial v}{\partial y} - \hat{\gamma}|V|\left(\frac{m}{V}\frac{dV}{dx}\frac{\partial h}{\partial x} + \frac{\partial^2 h}{\partial x^2} + \frac{\partial^2 h}{\partial y^2} \right) \right\} \tag{15}$$

The equations (13)-(15) allow for alongshore travelling and growing wave solutions of the form

$$(u,v,\eta,h) = \mathrm{Re}\{(\hat{u}(x),\hat{v}(x),\hat{\eta}(x),\hat{h}(x))e^{iky+\omega t}\} \tag{16}$$

Here k is the wavenumber and ω a complex frequency. The real part, $\mathrm{Re}(\omega)$, denotes the growth rate of the perturbation and $-\mathrm{Im}(\omega)$ the frequency. Instability occurs if $\mathrm{Re}(\omega)$ is positive: then the mode grows exponentially in time. The part which describes the bottom is called a topographic wave. As a result of (16), equations (13)-(15) can be written as an eigenvalue problem where ω is the eigenvalue and $h(x)$ the eigenfunction. The mathematical details and the solution procedure can be seen in Falqués et al. (1997), Falqués et al. (1998b).

3   Model Results

In this section the results obtained with the linear numerical model will be presented. In order to fit our model to the situation on the Dutch inner shelf, we choose values for the parameters L_V, L_H, U, r_*, and s as discussed in section 2.3. A value $\gamma = 0.08$ will be adopted for the Coulomb coefficient in the sediment flux. The Dutch coast is at a latitude of 51°N, thus the Coriolis parameter is $f_c = 1.12 \times 10^{-4}\,\text{s}^{-1}$. Consequently, the default values of the non-dimensional parameters in our study are

$$\hat{f} = 5.35 \qquad r = 1.5 \qquad \hat{\gamma} = 1 \times 10^{-4} \qquad \beta = 0.33 \qquad a = 0.23$$

In this study we will focuss on the dynamics of bedforms in the case where the current has the coast to the right in the Northern Hemisphere ($\hat{f} > 0, V < 0$), which is the case of the Dutch and the North American coasts. On the Argentinian shelf the current is directed to the north ($V > 0$ in the present model) but then, $\hat{f} < 0$. However, the latter situation is equivalent to the former one because the system has a mirror symetry with respect to the $y = 0$ plane, so that there are only two independent situations, $\hat{f}V < 0$ and $\hat{f}V > 0$. Some results for the latter case will also be presented when discussing the effect of Coriolis force.
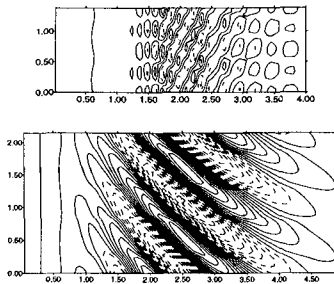
Figure 3: Bedforms for $m = 3$. See the text for explanation.

A sediment transport proportional to the current will be considered, i.e., $m = 1$. This choice is representative for situations where the wave-induced orbital velocity near the bed is much larger than the steady current. The sediment is then stirred by the waves and subsequently transported by the current. The effects of a sediment transport faster than linear, $m > 1$, have also been explored. In this case, the model gives bedforms different from the observed shoreface-connected ridges. These can be of two types: patches of alternate shoals and pools or cyclonically oriented ridges, see figure 3 up and down, respectively. The results in the case $m > 1$ can be seen in Falqués, Calvete & De Swart (1998a) and will be not further described here.

In figure 4 curves are presented of the growth rates of the first three eigenmodes for $a = 1$. In this case the basic state current is fully determined by the longshore pressure gradient. Note that the ratio V/H is constant, as was also studied by Trowbridge (1995). An important difference is that in the present model the preferred downslope movement of the sediment is accounted for. This causes the growth rate to have a maximum for $k \simeq 10$, which corresponds to a spacing
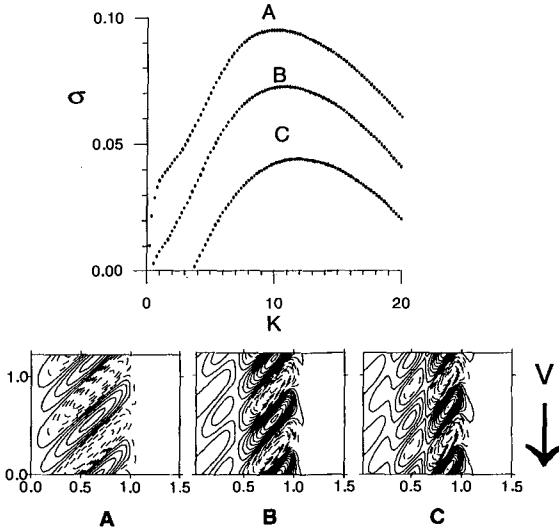
Figure 4: Nondimensional growth rate, $\sigma = \mathrm{Re}(\omega)$ as a function of the wavenumber, k, for the first three modes (upper part). Parameter values are $m = 1$, $a = 1$, $r = 1.5$, $\hat{f} = 5.35$, $\hat{\gamma} = 10^{-4}$, $\beta = 0.33$ and $V < 0$. The contour plots of the three bottom modes with the largest growth rate, are shown below. Crests and troughs are indicated by continuous and dashed lines, respectively. In each plot the y axis (vertical on the left) represents the shoreface and the $x > 0$ axis (horizontal on the bottom) the inner shelf. The direction of the basic current is shown by a big arrow. Note the upcurrent rotation of the ridges.

of about 7 km. This agrees with the observed spacings of shoreface-connected sand ridges on the Dutch inner shelf (Van de Meene, 1994). The corresponding phase speeds are $\simeq -1$ and this variable shows almost no dependence on k. This means that ridges behaves like topographic waves which migrate downcurrent with a celerity $V_{mi} \simeq L_H/T_m$. In view of the fact that the maximum growth rate is $\simeq 0.1$, the amplitude of the dominant bottom mode grows approximately 6% during the period that the pertubation travels one wave-length. An estimate of the characteristic growth time (e-folding time) can be obtained from the horizontal lengthscale, $L_H \sim 12$ km and a typical migration speed, $V_{mi} \sim 4\,\mathrm{m\,yr^{-1}}$, by means of $\tau = c L_H/V_{mi}\mathrm{Re}(\omega)$. This yields $\tau \sim 3 \times 10^4$ yr. The shape of the modelled ridges are shown in figure 4b. Clearly, the orientation of the dominant bedforms is such that they are upcurrent rotated: the seaward ends of the crests are shifted upstream with respect to their shoreface attachments. This agrees well with the observed orientation of the three ridge patches discussed in the introduction. Figure 5 shows the contour plot of mode 1 in figure 4 along with the corresponding perturbation on the current. The offshore deflection of the current over the crests and the onshore deflection over the troughs can be seen.

For $a < 1$, the longshore windstress contributes to the maintenance of the basic current profile and hence the ratio V/H is no longer constant. This leads to substantial differences compared with the case that $a = 1$. For a close to 1 the
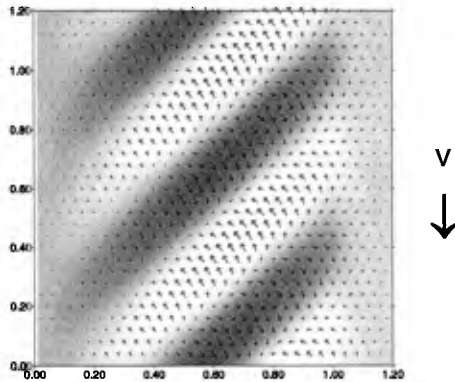
Figure 5: Contour plot of the first mode in figure 4 with the associated perturbation of the current indicated by arrows. Crests and troughs are indicated by dark and white colours, respectively. Note the offshore current deflection over the crests.

dominant wavenumber is close to 7, but with decreasing a this role is taken over by a much lower wavenumber, $k_m \sim 7$ for $a = 0.8$ and $k_m \sim 1$ for $a = 0.6$. Obviously, the predicted ridge spacings become much larger than those observed in the field. Besides, the growth rates decrease with decreasing a and hence the e-folding time scale of the bedforms becomes unrealistically large. Another interesting aspect is the competition between different modes with different spatial structures. The main differences are that some of them are attached to the shoreface while some are not. Sometimes they appear to be very elongated. Anyway, a striking overall characteristic of all modes is the upcurrent orientation of their crests.

The effect of earth rotation on the instability mechanism has been investigated by carrying out experiments with all parameters having their default values but for $a = 1$ and different values of the Coriolis parameter: $\hat{f} = 0, 7, -7$. The results, shown in figure 6, indicate that earth rotation hardly affects the topographic waves in the observed wavenumber range, $k \sim 10$. In this range, Coriolis force produces just an inshore shift of the ridges (C) in the Southern Hemisphere and an offshore shift in the Northern Hemisphere (A) along with a slight inhibition of the instability in the latter case. In contrast, earth rotation has a strong influence on long topographic waves, making the instability mechanism to be much more effective on the Southern Hemisphere. In this case, a sharp peak in the growth rate curve occurs for very long wave-lengths. The corresponding bedforms show a little obliquity with respect to the coast and differ substantially from the observed elongated ridges (D).

The sensitivity of the model results to the friction parameter has also been investigated. The general trend appears to be that growth rates increase with increasing r, in particular for relatively small wavenumbers ($k < 8$). However, for k around 10 or larger, the growth rates hardly depend on r. Furthermore, the wavenumber for which the instability mechanism is most effective become smaller if the friction parameter is increased. The shape of the preferred bottom modes do not change significantly.
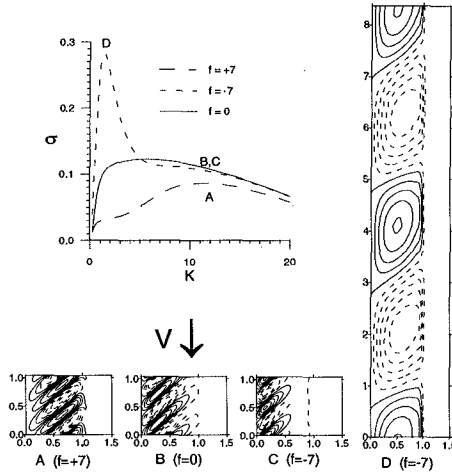
Figure 6: Growth rate curves of the first mode for different values of the Coriolis parameter $\hat{f}$. All other parameter values are $m = 1$, $a = 1$, $r = 1.5$, $\hat{\gamma} = 10^{-4}$, $\beta = 0.33$ and $V < 0$. The bottom contours are also shown, for $k = 12$ (A,B,C) and for the peak at $k = 1.5$ (D).

The bed slope β and the Coulomb coefficient $\hat{\gamma}$ have counteracting effects, the former de-stabilizing, the latter stabilizing. If $\hat{\gamma}$ becomes larger than about 8×10^{-4} instabilities do not longer exist.

4 Physical mechanisms

In this section the physical mechanisms which originate the formation of the ridges according to our model will be discussed. For this purpose it is useful to combine the continuity equation (14) and the bottom evolution equation (15) to obtain (in the quasi-steady limit $\epsilon \to 0$ and for small Froude number $F \to 0$)

$$
\frac{\partial h}{\partial t} + \frac{mq_0}{H}\frac{V}{|V|}\frac{\partial h}{\partial y} - \frac{\partial}{\partial x}\left(\hat{\gamma}q_0\frac{\partial h}{\partial x}\right) - \frac{\partial}{\partial y}\left(\hat{\gamma}q_0\frac{\partial h}{\partial y}\right) =
$$
$$
\frac{q_0}{|V|}\left(\frac{m}{H}\frac{dH}{dx} - \frac{(m-1)}{V}\frac{dV}{dx}\right)u + (m-1)\frac{q_0}{|V|}\frac{\partial u}{\partial x}
\tag{17}
$$

where $q_0 = |V|^m$. On the left-hand side an advective contribution and two diffusive terms appear. Thus, in absence of the right-hand side, this equation would describe just migrating and decaying bedforms. The principle sources for instability appear on the right-hand side. The first term only acts in case there is a transverse sloping reference bottom. The last two terms are only active in case $m > 1$ (i.e., a 'faster than linear' sediment transport parametrization).

Consider the first term on the right-hand side of equation (17). It shows that an offshore deflection over a bar $(u > 0)$ on a transverse sloping reference bottom causes a growth of the bar $(\partial h/\partial t > 0)$. This can be intuitively understood by considering a control volume at a crest (where $\partial/\partial y = 0$) with vertical sides

Offshore deflexion   Accretion
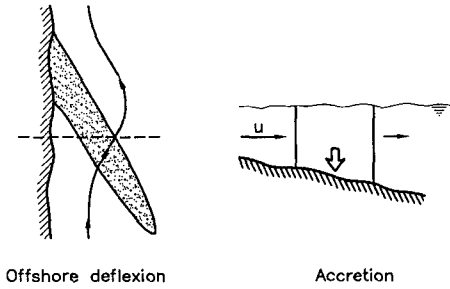
Figure 7: Schematic view of the transverse bottom slope mechanism. An upcurrent oriented ridge produces offshore deflection of the flow. Then, flow into deeper water must converge so that a sediment convergence occurs over the ridge.

parallel and perpendicular to the coast (see figure 7). In case of an offshore flow component ($u > 0$) the mass deficit caused by the movement of the column into deeper water must be compensated by a convergence of the flow. As the sediment flux, q, is proportional to a power of the velocity of the current, there will be convergence of sediment above the crests and thus the ridges will grow (see figure 7). Therefore, what we need now to explain the formation of the ridges is just a confirmation of the offshore deflection of the current over the crests. As a consequence of mass conservation in case of irrotational flow (Falqués et al., 1998a) it can be seen that an upcurrent oriented ridge causes an offshore deflection and that an downcurrent oriented ridge causes an inshore deflection. This is also confirmed by numerical simulation of the flow (see figure 5). Therefore, this behaviour achieves a positive feedback between bedforms and flow disturbance which is responsible for the growth of upcurrent oriented ridges.

The numerical simulation described in section 3 shows that the mechanism just explained is quite robust and that coriolis and frictional forces have only a moderate effect on it. What has a strong influence on the effectiveness of the transverse slope mechanism are the exponent m of the sediment transport and parameter $a = \delta/r$. The mechanism is most efficient for $m = 1$ and $a = 1$. This seems related to the fact that in this case the local migration celerity of the topographic waves, $m q_0/H$ (according to eq. (17)), is cross-shore uniform. Apparently, the cross-shore gradients on the migrational celerity inhibit the growth mechanism. The reason has not yet been fully understood.

In case of $m > 1$, and in conection with the last term in equation (17), two different instability mechanisms appear which are related to the production of vertical vorticity. The first one is caused by bottom frictional torques over an uneven sea bed and tends to produce patches of alternate shoals and pools (see figure 3). The second one comes from the stretching of planetary vorticity by an uneven sea bed and tends to originate elongated ridges which are cyclonically oriented (see figure 3). A detailed analysis of them can be seen in Falqués et al. (1998a).
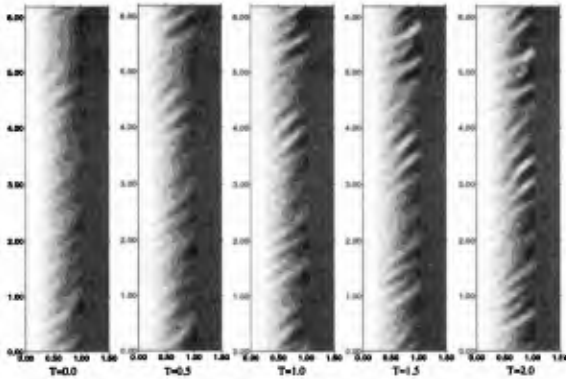
Figure 8: Nonlinear evolution. See explenations in the text.

5   Nonlinear model. Preliminary results

Nonlinear theory provides the tool for examining the long-term evolution of the shoreface-connected ridges into some form that is observable in the field. Following Schuttelaars (1997), the nonlinear solution is expanded in terms of the linear eigenfunctions. Time evolution equations are derived by inserting the expansion into the full nonlinear equations and then projecting the resulting equations onto the adjoint linear eigenfunctions. This Galerkin-type method has the considerable appeal of using actual linear solutions as a basis—rather than, say, some arbitrary polynomial—so that comparatively few terms are necessary to describe the non-linear evolution accurately. Work regarding the nonlinear equations is in progress. Figure 8 is shown as an example of some preliminary results. The time evolution of bathymetric contours from $t = 0$ to $t = 2$ (morphological time units) can be seen for $m = 1$, $a = 1$, $r = 1.5$, $\hat{f} = 5.35$. A number of 30 long-shore modes have been used, ranging from $k = 1$ to $k = 30$.

6   Conclusions

It has been shown that shoreface-connecte sand ridges are formed due to a positive feedback between the water motion and the erodible bottom. However, the results of the model depend essentialy on the sediment transport parametrization through the exponent m. In case $m = 1$ (sediment transport proportional to the current) the dominant bedforms are trapped to the inner shelf and they are elongated and upcurrent rotated. The growth rate and longshore spacing are largely determined by the relative contribution of wind and the longshore pressure gradient in the maintenance of the background current. In case the latter effect dominates the model results show good agreement with field data, e.g. in case of the Dutch inner shelf a spacing of about 7 km is obtained (see figure 1). With increasing wind effects the growth rates become smaller and the wave-lengths increase. Coriolis and bottom friction also affect the instability mechanism, but they do not induce significant qualitative changes. Physically, the bedforms are due to the transverse sloping bottom mechanism and their formation is associated with an offshore

current deflection over the bars. The mechanism is effective only for $1 \leq m < 1.05$.

If a larger exponent m in the sediment flux is considered other types of bottom modes are obtained which donot resemble the observed shoreface-connected ridges. They are generated by the coupling between topography and flow through the vorticity production due to an uneven sea bed either by frictional torques or by planetary vortex stretching.

It appears that the best comparison between model results and observed shoreface-connected ridges is obtained in case $m = 1$. A further condition is that the ratio V/H is almost constant, where V is the background current and H the equilibrium bottom profile, which is realistic if the background flow is mainly controlled by a longshore pressure gradient and not by the windstress. Thus, the present modeling provides a valuable information on the regions where shoreface-connected ridges occur: apparently, the long term averaged sediment transport is mainly due to wave stirring plus advection by the mean current which is in turn controlled by pressure gradients.

It is important to realize that observed shoreface-connected ridges on the inner shelf are finite amplitude features while the linear analysis only yields information on their initial formation. This limitation can be overcome by the nonlinear model which has been set up. Prelimany results reported here have proven to be promissing.

An examination of the large-scale bedforms in the map of the Southern Bight of the North Sea presented in figure 1.1 of (Van de Meene, 1994), suggests that the Dutch shoreface-connected ridges could very well be tidal sand banks just distorted by the proximity of the coast. However, the present study shows that shoreface-connected ridges have an entirely different origin. Indeed, tidal sand banks are associated to a $m > 1$ power in the sediment transport and to bottom friction, and their orientation depends on earth rotation (Hulscher et al., 1993). On the other hand, the observed orientation of the ridges is obtained only if $m \simeq 1$ and is not affected by Coriolis. Therefore, it is clear that the transverse slope mechanism is the main cause of the observed ridges and this has nothing to do with tidal oscillations. Nevertheless, it is conceivable that tidal currents affect the ridges in some way. To explore this possibility, an important extension of the present model consists in the assumption of a basic undisturbed current with a steady component plus an oscillatory one (tidal). This type of modelling is currently in progress and preliminary results are reported in Falqués et al. (1997).

Acknowledgements

References

CHASE, R. R. P. 1979 The coastal longshore pressure gradient: temporal variations and driving mechanisms. *J. Geophys. Res.* **84**, 4898–4904.

FALQUÉS, A., CALVETE, D. & DE SWART, H. E. 1997 Combined tidal and steady current model for shoreface-connected ridges. *Tech. Rep.* R97-4. IMAU, Utrecht Univ.

FALQUÉS, A., CALVETE, D. & DE SWART, H. E. 1998*a* Modelling the formation of shoreface-conected sand ridges: dynamic coupling between mean currents and topography. *J. Fluid Mech.* (submitted).

FALQUÉS, A., CALVETE, D. & MONTOTO, A. 1998*b* Bed-flow instabilities of coastal currents. In *Proc. 8th Biennal Conf. on Physics of Estuaries and Coastal Seas* (ed. J.Dronkers & M.Scheffers), pp. 417–424. A.A.Balkema. Rotterdam.

FREDSOE, J. & DEIGAARD, R. 1993 *Mechanics of coastal sediment transport.* World Scientific, Singapore.

HULSCHER, S. J. M. H., DE SWART, H. E. & DE VRIEND, H. J. 1993 The generation of offshore tidal sand banks and sand waves. *Cont. Shelf Res.* **13** (11), 1183–1204.

PARKER, G., LANFREDI, N. W. & SWIFT, D. J. P. 1982 Seafloor response to flow in a Southern Hemisphere sand-ridge field: Argentina inner shelf. *Sedimentary Geology* **33**, 195–216.

SCHUTTELAARS, H. M. 1997 Evolution and stability analysis of bottom patterns in tidal embayments. PhD thesis, Universiteit Utrech, Faculteit Wiskunde en Informatica.

SCOTT, J. T. & CSANADY, G. T. 1976 Nearshore currents off Long Island. *J. Geophys. Res.* **81**, 5401–5409.

SWIFT, D. J. P., NIEDORODA, A. W., VINCENT, C. E. & HOPKINS, T. S. 1985 Barrier island evolution, Middle Atlantic Shelf, U.S.A., part 1: shoreface dynamics. *Mar. Geol.* **63**, 331–361.

TROWBRIDGE, J. H. 1995 A mechanism for the formation and maintenance of shore-oblique sand ridges on storm-dominated shelves. *J. Geophys. Res.* **100** (C8), 16071–16086.

VAN DE MEENE, J. W. H. 1994 The shoreface connected ridges along the central Dutch coast. PhD thesis, Netherlands Geographical Studies, 174.

VAN DER GIESSEN, A., DE RUIJTER, W. P. M. & BORST, J. C. 1990 Three-dimensional current structure in the Dutch coastal zone. *Neth. J. Sea Res.* **25**, 45–55.

VAN RIJN, L. C. 1993 *Principles of sediment transport in rivers, estuaries and coastal seas..* Aqua Publ., Amsterdam.

ZIMMERMAN, J. T. F. 1981 Dynamics, diffusion and geomorphological significance of tidal residual eddies. *Nature* **290**, 549–555.